Title

Accelerated whole brain intracranial vessel wall imaging using black blood fast spin echo with compressed sensing (CS-SPACE)

Journal

Magnetic Resonance Materials in Physics, Biology and Medicine, 31(3)

ISSN

0968-5243

Authors

Zhu, Chengcheng
Tian, Bing
Chen, Luguang
et al.

Publication Date

2018-06-01

DOI

10.1007/s10334-017-0667-3

Peer reviewed

HHS Public Access

Author manuscript

MAGMA. Author manuscript; available in PMC 2018 June 01.

Published in final edited form as:

MAGMA. 2018 June ; 31(3): 457–467. doi:10.1007/s10334-017-0667-3.

Accelerated whole brain intracranial vessel wall imaging using black blood fast spin echo with compressed sensing (CS-SPACE)

Chengcheng Zhu[1], **Bing Tian**[2], **Luguang Chen**[2], **Laura Eisenmenger**[1], **Esther Raithel**[3], **Christoph Forman**[3], **Sinyeob Ahn**[4], **Gerhard Laub**[4], **Qi Liu**[2], **Jianping Lu**[2], **Jing Liu**[1], **Christopher Hess**[1], and **David Saloner**[1]

[1]Department of Radiology and Biomedical Imaging, University of California, San Francisco (UCSF), San Francisco, CA, USA

[2]Department of Radiology, Changhai Hospital, Shanghai, China

[3]Siemens Healthcare, Erlangen, Germany

[4]Siemens Healthcare, San Francisco, CA, USA

Abstract

Objective—Develop and optimize an accelerated, high-resolution (0.5 mm isotropic) 3D black blood MRI technique to reduce scan time for whole-brain intracranial vessel wall imaging.

Materials and methods—A 3D accelerated T_1-weighted fast-spin-echo prototype sequence using compressed sensing (CS-SPACE) was developed at 3T. Both the acquisition [echo train length (ETL), under-sampling factor] and reconstruction parameters (regularization parameter, number of iterations) were first optimized in 5 healthy volunteers. Ten patients with a variety of intracranial vascular disease presentations (aneurysm, atherosclerosis, dissection, vasculitis) were imaged with SPACE and optimized CS-SPACE, pre and post Gd contrast. Lumen/wall area, wall-to-lumen contrast ratio (CR), enhancement ratio (ER), sharpness, and qualitative scores (1–4) by two radiologists were recorded.

Results—The optimized CS-SPACE protocol has ETL 60, 20% *k*-space under-sampling, 0.002 regularization factor with 20 iterations. In patient studies, CS-SPACE and conventional SPACE had comparable image scores both pre- (3.35 ± 0.85 vs. 3.54 ± 0.65, $p = 0.13$) and post-contrast

Correspondence to: Chengcheng Zhu; Jianping Lu.

Author contributions Protocol/project development: CZ, SA, GL, ER, CF, JL, CH, DS. Data collection or management: CZ, LC, QL, JL. Data analysis: CZ, BT, LE.

Compliance with ethical standards

Conflict of interest Esther Raithel, Christoph Forman, Gerhard Laub and Sinyeob Ahn are employees of Siemens. Other authors declare that they have no conflict of interest.

Ethical approval All procedures performed in studies involving human participants were in accordance with the ethical standards of the institutional and/or national research committee and with the 1964 Helsinki declaration and its later amendments or comparable ethical standards. This study was conducted under IRB approval of the University of California San Francisco (reference number: 10-03248) and Changhai Hospital in Shanghai (reference number: CHEC2013-204).

Informed consent Informed consent was obtained from all individual participants included in the study.

Electronic supplementary material The online version of this article (https://doi.org/10.1007/s10334-017-0667-3) contains supplementary material, which is available to authorized users.

(3.72 ± 0.58 vs. 3.53 ± 0.57, $p = 0.15$), but the CS-SPACE acquisition was 37% faster (6:48 vs. 10:50). CS-SPACE agreed with SPACE for lumen/wall area, ER measurements and sharpness, but marginally reduced the CR.

Conclusion—In the evaluation of intracranial vascular disease, CS-SPACE provides a substantial reduction in scan time compared to conventional T_1-weighted SPACE while maintaining good image quality.

Keywords

3D black blood SPACE; Intracranial vessel wall MRI; Compressed sensing; Aneurysm; Atherosclerosis

Introduction

Intracranial vascular diseases, including atherosclerotic plaques and aneurysms, are major causes of ischemic or hemorrhagic strokes [1, 2]. The clinical management criteria for these diseases depends on imaging of the lumen, while the source of the disorder—the vessel wall—has rarely been considered. Recent capabilities of high resolution black blood MRI (hrMRI) have enabled the visualization of the intracranial vessel wall characteristics [3]. Several recent studies have demonstrated the ability of hrMRI to differentiate between different types of intracranial vascular disease [4], identify vulnerable atherosclerotic plaques [5–7] and recognize ruptured and unstable aneurysms [8].

Previously, imaging of the intracranial vessel wall was performed using 2D turbo-spin-echo hrMRI techniques [6, 8, 9]. Recently, variable flip-angle 3D fast-spin-echo sequences (such as Sampling Perfection with Application optimized Contrasts using different flip angle Evolution—SPACE) have been used by several groups to achieve high isotropic resolution (0.4–0.8 mm) suitable for visualizing vessel wall abnormalities. These provide improved visualization of the vessel wall and can achieve up to whole brain coverage [10–13]. However, even accelerated by traditional parallel imaging (PI) techniques (GRAPPA, SENSE and partial Fourier), these techniques still require long scan times (~ 10 min) for whole brain coverage, which are poorly tolerated by patients and are also vulnerable to motion artifacts.

Compressed sensing (CS) technique enables accelerated MRI by nonlinear iterative reconstruction of sparsely under-sampled *k*-space data [14, 15]. CS has been used to accelerate black blood extracranial T1 weighted carotid plaque imaging using 3D gradient echo sequences [16, 17], and also for the T2 mapping of the carotid plaque using a 3D fast-spin-echo (CUBE) technique [18]. The combination of CS and PI has also been used in different clinical applications, including the breast [19], carotid plaque [20], abdomen [21] and musculoskeletal disorders [22, 23].

To ensure that image artifacts are incoherent (noise-like), CS requires random sampling, although in practice, pseudo-random under-sampling is widely-accepted. Poisson-Disk sampling provides a homogeneous, random distribution of samples in *k*-space that is suitable for CS [24]. Previously, a CS-SPACE sequence was developed using a variable-density

Poisson-disc pattern for under-sampling, resulting in sixfold acceleration for imaging of the knee [23]. However, there has been little reported work for using CS for accelerated intracranial vessel wall imaging.

This study aims to evaluate and optimize CS for fast intracranial vessel wall imaging (VWI). We hypothesize that an optimized CS-SPACE approach will significantly reduce scan time while maintaining diagnostic image quality for the assessment of intracranial vascular diseases using high resolution acquisitions.

Materials and methods

Sequence design and imaging optimization

A T_1-weighted SPACE prototype sequence was used in this study for intracranial vessel wall imaging. The flip angle schedule was adopted from a previous study [10]. No additional blood suppression module was used, and the black blood effect was achieved by the variable flip angle train. It has been reported that high spatial resolution is required for reliable diagnosis of intracranial vascular diseases; therefore this study utilized an isotropic resolution of 0.5 mm [11].

Poisson-disc variable density acquisition with elliptical *k*-space coverage was used. The center of *k*-space was fully sampled to allow computation of a coil sensitivity map for image reconstruction [23]. A fully sampled *k*-space center of size 24 × 24 was used for coil sensitivity map estimation in this work. The binary undersampling mask is shown in Fig. 1.

The reconstruction used in this paper combines CS and PI by minimizing the following cost function as described in [23]:

$$\hat{x} = \arg\min_{x} \frac{1}{2} \sum_{n=1}^{N} y_n - F_u\left(\mathrm{CSM}_n \odot x\right)_2^2 + \lambda W x_1,$$

$\hat{x}$ being the image to be reconstructed. In the first term, the data fidelity term that ensures data consistency, N is the number of receive channels of the coil, Y_N is the N-th raw data channel, F_U the undersampled Fourier transform, and CSM_N the respective coil sensitivity map. In the second term, the regularization term, sparsity of the solution is promoted in the wavelet domain by penalizing the L1 norm of W_X. The regularization parameter λ balances between smoothness and the reduction of noise and aliasing artifacts. The under-sampling factor can be chosen freely. PI was used for the full acquisition of the center of *k*-space in order to determine the coil sensitivity map.

For intracranial vessel wall imaging, under-sampling is challenging because the imaging target—the vessel walls—are extremely thin structures that require reproduction of high frequency information in *k*-space for accurate depiction. In order to evaluate and optimize compressed sensing for intracranial vessel wall imaging, the acquisition parameters (ETL and under-sampling factor) and reconstruction parameters (regularization parameters and number of iterations) were optimized using the following approach in 5 volunteers: (1) the ETL was fixed at 60, then under-sampling factors of 14, 17 and 20% were evaluated. The

choice of these factors was based on preliminary experiments which showed a factor below 14% produced unsatisfactory image quality. (2) Three combinations of ETL and under-sampling factors (ETL60 20%; ETL50 16.5%; ETL40 14%) were performed at a fixed scan time for fair comparative evaluation. The choice of ETLs was based on previous studies [5, 10, 12]. An ETL longer than 60 can cause significant blurring, and an ETL shorter than 40 is not time efficient. Scanning protocols are listed in Table 1. When optimizing acquisition parameters, reconstruction parameters were set empirically to use a regularization parameter of 0.002 and 20 iterations. Once the optimized ETL and under-sampling factor (which provided the best image quality) were determined, regularization parameters of 0.0005, 0.001, 0.002 and 0.004 were evaluated (number of iterations was fixed at 40). The influence of 10, 20, 30 and 40 iterations were also evaluated.

Study population

Five healthy volunteers (4 male, age 31.8 ± 6.3) without intracranial vascular disease and 10 patients (6 male, age 55.3 ± 18.1) with intracranial vascular diseases were recruited from two centers. All volunteers were recruited at the University of California San Francisco (UCSF). Seven patients were recruited at UCSF, and 3 patients were from Changhai Hospital, Shanghai, China. Sixteen intracranial vascular lesions were identified in 10 patients, including 11 aneurysms [7 internal carotid artery (ICA), three middle cerebral artery (MCA), and one anterior communicating artery (AComm)], three atherosclerotic plaques [two vertebral artery (VA) plaque, one VA occlusion], one VA dissection and one ICA-MCA vasculitis. This study was conducted under local IRB approval of UCSF (reference number: 10-03248) and Changhai Hospital in Shanghai (reference number: CHEC2013-204). All subjects involved gave informed written consent for study participation.

MR imaging

Subjects were scanned on 3T Siemens Skyra scanners using standard 20 channel phased-array head and neck coils. A T1 SPACE protocol with conventional acceleration (GRAPPA 2 in phase direction, 6/8 partial Fourier in slice direction and elliptical *k*-space sampling) was used [10]. Non-selective 90° excitation pulses were used. Images were acquired in the sagittal plane with whole brain coverage and 0.5 mm isotropic resolution. The frequency encoding direction was head to feet, and phase encoding directions were anterior–posterior and left–right. A flip down pulse module at the end of the refocusing RF pulse train was used to improve the T1 contrast of the vessel wall [12]. The protocol was optimized on volunteers scanned using CS-SPACE protocols with different ETLs and under-sampling factors. SPACE and CS-SPACE parameters that were used in the optimization are listed in Table 1. Patients were scanned with SPACE (ETL 60) and the optimized CS-SPACE (ETL 60 and 20% under-sampling) protocols, both pre- and post-Gd injection. The CS reconstruction was implemented in-line on the scanner with a computation time of 3–12 min, depending on the number of iterations. Reconstruction was performed in the background while other acquisitions were running.

Acquisition with a 0.6 mm isotropic resolution CS-SPACE protocol (ETL 60, 20% under-sampling, scan time 4:08 s) was also evaluated in four patients (one with vertebral

dissection, one with vertebral occlusion, one with two MCA aneurysms, and one with MCA-ICA vasculitis), and the image quality was reviewed both pre- and post-contrast.

Image analysis

Images with strong motion artifacts were excluded in the analysis. Qualitative image quality was evaluated by experienced radiologists (BT, LE and CH) using a four-point scale.

Score 1: Vessel wall not seen clearly; poor image quality.

Score 2: Vessel wall seen in part; diagnostic image quality.

Score 3: Vessel wall seen clearly in most parts; good image quality.

Score 4: Sharp vessel wall confidently delineated; excellent image quality.

Because *k*-space under-sampling is intrinsically anisotropic in that data is only under-sampled along phase-encoding directions, the image quality was evaluated in specific imaging planes (sagittal, coronal or axial). For the volunteer scans, the image quality of the MCA (in the sagittal plane), ICA (in the sagittal plane and the axial plane), basilar artery (in the axial plane) were separately evaluated by a radiologist (BT), blinded to the different sequences used. The image quality of different CS-SPACE protocols was compared with that of original SPACE, and the best protocol was determined.

For the patient studies, image quality was evaluated using 3D multi-planar reconstruction in order to best visualize lesions of interest. Each lesion was independently assigned an image score by two radiologists (LE and CH), blinded to the image sequences used. Both pre- and post-contrast images were evaluated. Each radiologist also independently reviewed the vessel wall enhancement (dichotomized as either YES or NO) after contrast injection.

In the volunteer study, three continuous slices from the center of the MCA M1 segment (in the sagittal plane), the ICA C2 segment (in the axial plane) and the middle of the basilar artery (in the axial plane) were chosen for quantitative analysis. The lumen and outer wall boundaries were manually drawn in both SPACE and CS-SPACE sequences using Osirix software (Pixmeo, Switzerland). The lumen area, wall area and wall to lumen contrast ratio ($CR_{wall/lumen}$ = signal of wall/signal of lumen) were calculated. Area measurements from each CS-SPACE protocol were compared with SPACE. The protocol with best agreement and highest $CR_{wall/lumen}$ was determined.

In the patient study, quantitative analysis was performed on 3 continuous slices from each lesion. For patients with atherosclerotic disease, these slices were centered at the location of maximal plaque area; for patients with aneurysmal disease, these slices were centered at the location of maximal aneurysm diameter. The evaluated slices were placed perpendicular to the central line of the vessel. For the patient with ICA-MCA vasculitis, three slices at the middle of MCA M1 segment were used. The lumen and wall areas and $CR_{wall/lumen}$ were measured and calculated and compared between CS-SPACE and SPACE. The sharpness of the vessel wall inner/outer boundaries was measured using a method previously defined [25] using Micro View software (Parallax Innovations Inc., Ontario, Canada). The images were first interpolated by a factor of 10. Two straight orthogonal lines were drawn perpendicular to the vessel boundaries and the line intensity profiles were generated. These two lines were

anterior–posterior and inferior-superior for MCA or anterior communicating artery (in oblique sagittal planes) and anterior–posterior and left–right for ICA/basilar artery/vertebral artery (in axial planes). Based on the profile, the sharpness was defined as: sharpness = $1/d$, where d is the distance between positions of 20 and 80% of the difference of maximum and minimum intensity values (in mm) [25]. Quantitative analysis of patient images was performed on both pre- and post-contrast images. The enhancement of the vessel wall was quantified as enhancement ratio (ER): signal of vessel wall post-contrast/signal of vessel wall pre-contrast. The ERs measured on CS-SPACE was compared against SPACE as a reference standard.

Statistical analysis

Normality assumptions were formally assessed using the Shapiro–Wilk's test. Distributions were summarized using the median [inter-quartile range (IQR)] or the mean ± standard deviation (SD). Paired student t tests or Wilcoxon signed rank paired test were used to compare measurements from two methods. ANOVA was used to compare measurements from multiple protocols. Intraclass correlation coefficient (ICC) was used to test the agreement of two measurements. A 2-sided p value of less than 0.05 was considered significant. GraphPad prism 5 (GraphPad Software Inc., CA, USA) and R Statistics (version 3.1.3, www.r-project.org) were used for statistical analyses.

Results

Optimization of CS-SPACE

Sample images obtained during optimization of acquisition parameters in a healthy volunteer's basilar artery are shown in Fig. 2. ETL60-20% and ETL50-16.5% had the best image quality compared with other CS-SPACE protocols. The qualitative image scores of SPACE and different CS-SPACE protocols are shown in Table 2, and the bar plots are shown in supplemental Figure S1. The CS-SPACE protocols with best image quality were ETL60-20% (image score 3.08 ± 0.57) and ETL50-16.5% (3.14 ± 0.65); however, their image scores were still slightly lower than those for SPACE (3.46 ± 0.76). There was no significant difference between the scores of ETL60-20% and ETL50-16.5% ($p = 0.56$). Both SPACE and optimized CS-SPACE achieved good image quality (average scores > 3). Optimized CS-SPACE protocols reduced total scan time by 37–38% compared with conventional SPACE. When the ETL was fixed, the reduction of k-space sampling from 20 to 14% reduced the image quality of CS-SPACE. When the under-sampling factor was fixed (14 or 17%), a shorter ETL improved the image quality, at the cost of increased scan time. Of the different vascular beds, the MCA demonstrated the best image quality, while the basilar artery had the lowest image quality. For the ICA, the image quality in the sagittal plane was significantly higher than that in the axial plane.

The quantitative measurements of areas/contrast ratios are shown in Table 3. There was no significant difference between SPACE and CS-SPACE for lumen area measurements ($p = 0.18$). The ETL60-20% and ETL50-16% had comparable outer area ($p = 0.48$ and 0.78, respectively) and wall area measurements ($p = 0.98$ and 0.55, respectively) compared with SPACE. However, ETL60-17%, ETL60-14% and ETL40-14% overestimated the outer area

and wall area ($p < 0.01$). CS-SPACE protocols had slightly higher contrast ratio compared with SPACE ($p = 0.007$). ETL60-20% had the best agreement of vessel area measurement compared with SPACE with an average ICC of 0.89. Together with the consideration of the image score, ETL60-20% was chosen as the optimized CS-SPACE protocol.

Images of the basilar artery in a volunteer are shown with different regularization factors in Fig. 3. The radiologists determined that a regularization factor of 0.002 was optimal for visual review. The radiologists also found that there were no visual differences among images with a number of iterations from 10 to 40. The reconstruction times for 10–40 iterations were 3, 6, 9 and 12 min. Therefore, to limit reconstruction time, the number of iterations was set to 10. The in-line reconstruction time for the optimized protocol was 3 min.

Patient studies

Of the 10 patients included in the study, eight completed the full MRI examination. One aneurysm patient did not have CS-SPACE scans pre-contrast due to limited time. In total, there were 19 pairs of SPACE and CS-SPACE data sets available for comparison (9 pairs of pre-contrast and 10 pairs of post-contrast). No patient had an image score of 1 (non-diagnostic), so no imaging dataset was excluded in the analysis. Sample images of patients with vasculitis, dissection andaneurysms are shown in Figs. 4, 5, and 6, respectively.

Qualitative rating of SPACE and CS-SPACE images for each lesion are shown in Table 4. Both SPACE and CS-SPACE achieved good image quality for the average (score > 3). CS-SPACE had comparable image quality compared to SPACE, both pre- and post-contrast ($p > 0.05$). The two reviewers had good agreement for image scoring [ICC (95% CI) = 0.765 (0.584, 0.868)]. Both radiologists identified vessel wall enhancement in 13 of 16 lesions, and there was perfect agreement between radiologists and between sequences. Quantitative vessel areas, contrast ratio, and sharpness measurements of SPACE and CS-SPACE are summarized in Table 5. CS-SPACE had comparable lumen/wall area measurements, vessel wall sharpness and enhancement ratio with SPACE ($p > 0.05$), but had a slightly lower wall/lumen contrast ratio ($p = 0.02$). There was excellent agreement of vessel area and enhancement ratio measurements between sequences (ICCs > 0.89).

Sample images of 0.6 mm isotropic CS-SPACE are shown in Fig. 4. The 0.6 mm CS-SPACE protocol had overall lower image quality compared to CS-SPACE 0.5 mm or SPACE 0.5 mm (image scores in 4 patients: 3.50 ± 0.53 vs. 4.00 ± 0.00 and 4.00 ± 0.00, respectively), but still achieved good diagnostic image quality on average (> 3). All cases of contrast enhancement were detected on 0.6 mm CS-SPACE.

Discussion

To our best knowledge, this is the first study that applies compressed sensing to 3D black blood intracranial vessel wall imaging. The acquisition and reconstruction parameters for CS-SPACE were optimized. With the optimized sequences, the feasibility of using these acceleration methods was demonstrated in a small group of patients with variable intracranial vascular diseases. The optimized CS-SPACE showed comparable image quality

and reliable measurements of vessel areas and contrast enhancement when compared to SPACE, with a scan time reduction of 37%. Using CS-SPACE, 0.5 mm isotropic resolution intracranial vessel wall imaging with whole brain coverage was feasible in less than 7 min.

Imaging and quantification of the intracranial vessel wall characteristics is technically demanding because: (1) the combined thickness of the intima, media and adventitia of the intracranial arteries is small (< 0.5 mm in the absence of disease [26]): (2) the anatomy of the intracranial arteries rarely fits standard anatomic planes; and, (3) it is challenging to generate sufficient contrast between vessel wall and surrounding blood/cerebrospinal fluid/brain parenchyma. Three-dimensional fast-spin-echo T1 with variable flip angle acquisition has been proposed as a promising tool for intracranial vessel wall imaging given its high scan efficiency, high isotropic resolution (0.4 to 0.8 mm) and intrinsic black blood effect [11, 27]. However, acquiring such a high resolution 3D dataset often requires a scan time of ~ 10 min. A post-contrast scan is also required, which further lengthens the scan time. These long scan times are poorly tolerated by patients, especially symptomatic patients following a stroke or TIA. Lengthy scan times also increase the incidence of motion-related artifacts, which increase the failure rates of MRI studies [28]. The CS-SPACE method used in this study significantly reduces scan time (by more than 1/3) while maintaining excellent image quality. It improves patient comfort, reduces cost, and has the potential of improving the successful rate of MRI exams. It may facilitate the use of 3D intracranial vessel wall imaging in a clinical setting.

Our preliminary test of a 0.6 mm isotropic resolution CS-SPACE protocol also showed good image quality and characterization of vessel wall enhancement in a scan time as short as 4 min. In the clinical setting, most MRI sequences are shorter than 5 min. Therefore, this protocol has high potential for use in routine clinical scans. Such results, although promising, need to be interpreted with caution since reduced resolution may negatively influence the evaluation and quantification of vascular disease. A previous study showed that a reduction of resolution in 3D fast-spin-echo (from 0.4 to 0.5 mm) might cause a highly stenotic intracranial artery to appear totally occluded because of partial volume effects of the narrowed lumen [11]. However, lower resolution may be sufficient for evaluating certain vessel wall characteristics, for example, the size of large intracranial aneurysms and the wall enhancement pattern in vasculitis. Ideally, an optimized imaging resolution should be chosen based on the specific application, with a balance between diagnostic performance and scan time. Our proposed compressed sensing method can reduce the scan time regardless of the resolution.

The CS approach has benefits over traditional PI methods. To match the acceleration factor of CS-SPACE (5 in this study) using conventional imaging, a GRAPPA/SENSE acceleration of 2 × 2 (together with elliptical scanning) is needed. The use of such high acceleration factors significantly reduces SNR and results in poor image quality. A sample image using GRAPPA 2 × 2 and elliptical scanning in a healthy volunteer is shown in supplemental Figure S2; significantly lower SNR is clearly apparent. In contradistinction, our study shows that CS-SPACE maintains good SNR with an acceleration factor of 5.

A standard 20-channel head coil was used in this study. The use of 32 channel or 64 channel head coils has potential to further improve the image quality. Although Poisson-Disk has been accepted as an efficient algorithm for generating random under-sampling patterns, several methods, including our previously developed method CIRCUS [29], have been developed for providing smoother transitions in the view ordering, especially for gradient echo sequences, that help avoid eddy current errors.

Online reconstruction was implemented on the scanner and GPU computing was enabled. Reconstruction of the optimized protocol took only 3 min and, as it ran in the background, it did not interrupt continued scanning. These features would facilitate the use of CS-SPACE in the clinical setting.

Similar to previous whole brain studies [10, 12], images were acquired in the sagittal plane. Thus, *k*-space was under-sampled only in the two phase encoding directions (left–right and anterior–posterior). The anisotropic under-sampling led to different image quality degradation in different imaging planes. Images in the axial plane had the worst image quality because both directions were undersampled. As the BA/VA vessel wall was best visualized in the axial plane, CS-SPACE had relatively lower image quality for the evaluation of BA/VA compared to other arteries. For the evaluation of a specific vessel, the choice of the frequency encoding direction should be considered for optimized image quality.

Contrast enhancement is associated with an increased risk of stroke symptoms [5]. We found CS-SPACE can reliably characterize and quantify contrast enhancement of the vessel wall. CS-SPACE can also reliably quantify vessel areas, and can potentially replace SPACE for the quantitative measurement of intracranial wall features.

In this study, we evaluated only T_1-weighted imaging techniques. Other groups have reported 3D multi-contrast intracranial vessel wall imaging (T_1-, T_2- and proton density weighted) [30, 31], however, at a much lower resolution (0.8 mm isotropic, 4 times of voxel size compared with the current study 0.5 mm isotropic). To achieve high isotropic resolution in T2 weighted imaging is challenging, given the longer TR (> 2000 ms) and the blurring caused by long ETLs (around 100). Future study is needed to evaluate the performance of CS for T_2-weighted fast-spin-echo imaging.

As can be observed in the figures, residual ripple-like artifacts and slightly differing contrast are present in some CS-SPACE images. Although such artifacts were mostly not in the vessel wall, limitations of the compressed sensing undersampling need to be recognized. The reconstruction had a SENSE component (the data fidelity term, with explicit use of the coil sensitivities), thus aliasing artifacts occurred in cases where the FOV was not sufficiently large. In some of our patients this was the case and induced ripple-like artifacts (for example in Fig. 6). This limitation of the reconstruction algorithm that was used in this paper can be overcome by using the ESPIRiT approach [32]. The different contrast may also be partially attributed to the actual *k*-space trajectory. Both SPACE and CS-SPACE used Cartesian sampling with radial-like reordering, i.e., each echo train went through the center of k space.

However, the variable density sampling pattern of the *k*-space in CS-SPACE, and the differences in the actual reorderings, could lead to slight contrast differences.

To our knowledge, there have not been studies applying compressed sensing for intracranial black blood vessel wall imaging. Previous compressed sensing vessel wall studies have focused on carotid plaque imaging, including plaque morphology imaging using 3D gradient echo sequences with black blood preparation [16] or 3D fast spin echo sequences (CUBE) [20] and T2 mapping [18]. Makhijani et al. used a hidden Markov tree model based compressing method for carotid plaque imaging using a diffusion prepared gradient echo sequence (MERGE), and found that a 4.5-fold acceleration achieved imaging quality comparable to a fully sampled reference in 6 patients with carotid diseases [16], which is comparable with the optimized acceleration factor in this study (fivefold). Yuan et al. investigated a compressed sensing based 3D multi-contrast fast-spin-echo imaging of the carotid plaque in 12 volunteers and 8 patients [18]. The sequence they used (CUBE) is comparable with the sequence in this study (SPACE). Although they reported CS-CUBE had good agreement with full sampled CUBE in carotid wall area measurements, they achieved an acceleration factor of only 1.5 or 2, which provided only a limited reduction in scan time.

There are a number of limitations in this study. First, the technique was evaluated in only a small number of patients. Specifically, very few patients were enrolled with atherosclerosis, dissection or vasculitis. CS-SPACE needs to be evaluated in a larger number of patients to prove its clinical feasibility for the diagnosis of intracranial vascular diseases. Second, there is a lack of a gold standard for measuring vessel wall dimensions. A resolution phantom will be useful to assess the accuracy of the techniques. Third, other *k*-space sampling patterns were not tested and compared in this study, and future studies of those approaches are warranted. Fourth, we did not optimize the 0.6 mm CS-SPACE protocol. Due to the different SNR, resolution and matrix compared with the 0.5 mm protocol, the optimized parameters could be different. However, the fast 4 min protocol we proposed in this study was only a proof of concept. Optimization of the imaging resolution and CS-SPACE parameters should be evaluated in the future for specific clinical applications.

Conclusion

CS-SPACE can achieve high resolution, isotropic, whole brain intracranial vessel wall imaging with acceptable image quality compared to SPACE, while significantly reducing the scan time. This technique has the potential for use in the clinical setting in the evaluation of patients with cerebral vascular diseases.

Supplementary Material

Refer to Web version on PubMed Central for supplementary material.

Acknowledgments

This study is supported by National Institute of Health (NIH) Grants R01HL114118, R01NS059944 and K99HL136883.

References

1. Gorelick PB, Wong KS, Bae HJ, Pandey DK. Large artery intracranial occlusive disease: a large worldwide burden but a relatively neglected frontier. Stroke J Cereb Circ. 2008; 39(8):2396–2399.
2. Brown RD Jr, Broderick JP. Unruptured intracranial aneurysms: epidemiology, natural history, management options, and familial screening. Lancet Neurol. 2014; 13(4):393–404. [PubMed: 24646873]
3. Mandell DM, Mossa-Basha M, Qiao Y, Hess CP, Hui F, Matouk C, Johnson MH, Daemen MJ, Vossough A, Edjlali M, Saloner D, Ansari SA, Wasserman BA, Mikulis DJ. Intracranial vessel wall MRI: principles and expert consensus recommendations of the American Society of Neuroradiology. AJNR Am J Neuroradiol. 2017; 38(2):218–229. [PubMed: 27469212]
4. Mossa-Basha M, Hwang WD, De Havenon A, Hippe D, Balu N, Becker KJ, Tirschwell DT, Hatsukami T, Anzai Y, Yuan C. Multicontrast high-resolution vessel wall magnetic resonance imaging and its value in differentiating intracranial vasculopathic processes. Stroke. 2015; 46(6): 1567–1573. [PubMed: 25953365]
5. Qiao Y, Zeiler SR, Mirbagheri S, Leigh R, Urrutia V, Wityk R, Wasserman BA. Intracranial plaque enhancement in patients with cerebrovascular events on high-spatial-resolution MR images. Radiology. 2014; 271(2):534–542. [PubMed: 24475850]
6. Yu JH, Kwak HS, Chung GH, Hwang SB, Park MS, Park SH. Association of intraplaque hemorrhage and acute infarction in patients with basilar artery plaque. Stroke. 2015; 46(10):2768–2772. [PubMed: 26306752]
7. Kim JM, Jung KH, Sohn CH, Moon J, Shin JH, Park J, Lee SH, Han MH, Roh JK. Intracranial plaque enhancement from high resolution vessel wall magnetic resonance imaging predicts stroke recurrence. Int J Stroke. 2016; 11(2):171–179. [PubMed: 26783308]
8. Edjlali M, Gentric JC, Regent-Rodriguez C, Trystram D, Hassen WB, Lion S, Nataf F, Raymond J, Wieben O, Turski P, Meder JF, Oppenheim C, Naggara O. Does aneurysmal wall enhancement on vessel wall MRI help to distinguish stable from unstable intracranial aneurysms? Stroke. 2014; 45(12):3704–3706. [PubMed: 25325912]
9. Teng Z, Peng W, Zhan Q, Zhang X, Liu Q, Chen S, Tian X, Chen L, Brown AJ, Graves MJ, Gillard JH, Lu J. An assessment on the incremental value of high-resolution magnetic resonance imaging to identify culprit plaques in atherosclerotic disease of the middle cerebral artery. Eur Radiol. 2016; 26(7):2206–2214. [PubMed: 26376883]
10. Zhu C, Haraldsson H, Tian B, Meisel K, Ko N, Lawton M, Grin-stead J, Ahn S, Laub G, Hess C, Saloner D. High resolution imaging of the intracranial vessel wall at 3 and 7 T using 3D fast spin echo MRI. Magma. 2016; 29(3):559–570. [PubMed: 26946509]
11. Qiao Y, Steinman DA, Qin Q, Etesami M, Schar M, Astor BC, Wasserman BA. Intracranial arterial wall imaging using three-dimensional high isotropic resolution black blood MRI at 3.0 Tesla. J Magn Reson Imaging JMRI. 2011; 34(1):22–30. [PubMed: 21698704]
12. Fan Z, Yang Q, Deng Z, Li Y, Bi X, Song S, Li D. Whole-brain intracranial vessel wall imaging at 3 Tesla using cerebrospinal fluid-attenuated T1-weighted 3D turbo spin echo. Magn Reson Med. 2017; 77(3):1142–1150. [PubMed: 26923198]
13. Harteveld AA, van der Kolk AG, van der Worp HB, Dieleman N, Siero JC, Kuijf HJ, Frijns CJ, Luijten PR, Zwanenburg JJ, Hendrikse J. High-resolution intracranial vessel wall MRI in an elderly asymptomatic population: comparison of 3T and 7T. Eur Radiol. 2017; 27(4):1585–1595. [PubMed: 27387876]
14. Candes E, Romberg J, Tao T. Robust uncertainty principles: exact signal reconstruction from highly incomplete frequency information. IEEE Trans Inf Theory. 2006; 52(2):489–509.
15. Lustig M, Donoho D, Pauly JM. Sparse MRI: the application of compressed sensing for rapid MR imaging. Magn Reson Med. 2007; 58(6):1182–1195. [PubMed: 17969013]
16. Makhijani MK, Balu N, Yamada K, Yuan C, Nayak KS. Accelerated 3D MERGE carotid imaging using compressed sensing with a hidden Markov tree model. J Magn Reson Imaging JMRI. 2012; 36(5):1194–1202. [PubMed: 22826159]

17. Li B, Dong L, Chen B, Ji S, Cai W, Wang Y, Zhang J, Zhang Z, Wang X, Fang J. Turbo fast three-dimensional carotid artery black-blood MRI by combining three-dimensional MERGE sequence with compressed sensing. Magn Reson Med. 2013; 70(5):1347–1352. [PubMed: 23280949]
18. Yuan J, Usman A, Reid SA, King KF, Patterson AJ, Gillard JH, Graves MJ. Three-dimensional black-blood T2 mapping with compressed sensing and data-driven parallel imaging in the carotid artery. Magn Reson Imaging. 2017; 37:62–69. [PubMed: 27888153]
19. Feng L, Grimm R, Block KT, Chandarana H, Kim S, Xu J, Axel L, Sodickson DK, Otazo R. Golden-angle radial sparse parallel MRI: combination of compressed sensing, parallel imaging, and golden-angle radial sampling for fast and flexible dynamic volumetric MRI. Magn Reson Med. 2014; 72(3):707–717. [PubMed: 24142845]
20. Yuan, J., Usman, A., Reid, SA., King, KF., Patterson, AJ., Gillard, JH., Graves, MJ. Three-dimensional black-blood multi-contrast carotid imaging using compressed sensing: a repeatability study. Magn Reson Mater Phy. 2017. https://doi.org/10.1007/s10334-017-0640-1
21. Seo N, Park MS, Han K, Kim D, King KF, Choi JY, Kim H, Kim HJ, Lee M, Bae H, Kim MJ. Feasibility of 3D navigator-triggered magnetic resonance cholangiopancreatography with combined parallel imaging and compressed sensing reconstruction at 3T. J Magn Reson Imaging JMRI. 2017; 46(5):1289–1297. [PubMed: 28295827]
22. Pandit P, Rivoire J, King K, Li X. Accelerated T1rho acquisition for knee cartilage quantification using compressed sensing and data-driven parallel imaging: a feasibility study. Magn Reson Med. 2016; 75(3):1256–1261. [PubMed: 25885368]
23. Fritz J, Raithel E, Thawait GK, Gilson W, Papp DF. SixFold acceleration of high-spatial resolution 3D SPACE MRI of the knee through incoherent *k*-space undersampling and iterative reconstruction-first experience. Invest Radiol. 2016; 51(6):400–409. [PubMed: 26685106]
24. Li G, Hennig J, Raithel E, Buchert M, Paul D, Korvink JG, Zaitsev M. An L1-norm phase constraint for half-Fourier compressed sensing in 3D MR imaging. Magma. 2015; 28(5):459–472. [PubMed: 25712732]
25. Larson AC, Kellman P, Arai A, Hirsch GA, McVeigh E, Li D, Simonetti OP. Preliminary investigation of respiratory self-gating for free-breathing segmented cine MRI. Magn Reson Med. 2005; 53(1):159–168. [PubMed: 15690515]
26. Jiang Y, Zhu C, Peng W, Degnan AJ, Chen L, Wang X, Liu Q, Wang Y, Xiang Z, Teng Z, Saloner D, Lu J. Ex-vivo imaging and plaque type classification of intracranial atherosclerotic plaque using high resolution MRI. Atherosclerosis. 2016; 249:10–16. [PubMed: 27062404]
27. Zhu C, Sadat U, Patterson AJ, Teng Z, Gillard JH, Graves MJ. 3D high-resolution contrast enhanced MRI of carotid atheroma—a technical update. Magn Reson Imaging. 2014; 32(5):594–597. [PubMed: 24630443]
28. Boussel L, Arora S, Rapp J, Rutt B, Huston J, Parker D, Yuan C, Bassiouny H, Saloner D. Atherosclerotic plaque progression in carotid arteries: monitoring with high-spatial-resolution MR imaging—multicenter trial. Radiology. 2009; 252(3):789–796. [PubMed: 19508991]
29. Liu, J., Feng, L., Shen, HW., Zhu, C., Wang, Y., Mukai, K., Brooks, GC., Ordovas, K., Saloner, D. Highly-accelerated self-gated free-breathing 3D cardiac cine MRI: validation in assessment of left ventricular function. Magn Reson Mater Phy. 2017. https://doi.org/10.1007/s10334-017-0646-8
30. Xu Y, Yuan C, Zhou Z, He L, Mi D, Li R, Cui Y, Wang Y, Wang Y, Liu G, Zheng Z, Zhao X. Co-existing intracranial and extracranial carotid artery atherosclerotic plaques and recurrent stroke risk: a three-dimensional multicontrast cardiovascular magnetic resonance study. J Cardiovasc Magn Reson Off J Soc Cardiovasc Magn Reson. 2016; 18(1):90.
31. Zhou Z, Li R, Zhao X, He L, Wang X, Wang J, Balu N, Yuan C. Evaluation of 3D multi-contrast joint intra- and extracranial vessel wall cardiovascular magnetic resonance. J Cardiovasc Magn Reson Off J Soc Cardiovasc Magn Reson. 2015; 17:41.
32. Uecker M, Lai P, Murphy MJ, Virtue P, Elad M, Pauly JM, Vasanawala SS, Lustig M. ESPIRiT—an eigenvalue approach to autocalibrating parallel MRI: where SENSE meets GRAPPA. Magn Reson Med. 2014; 71(3):990–1001. [PubMed: 23649942]

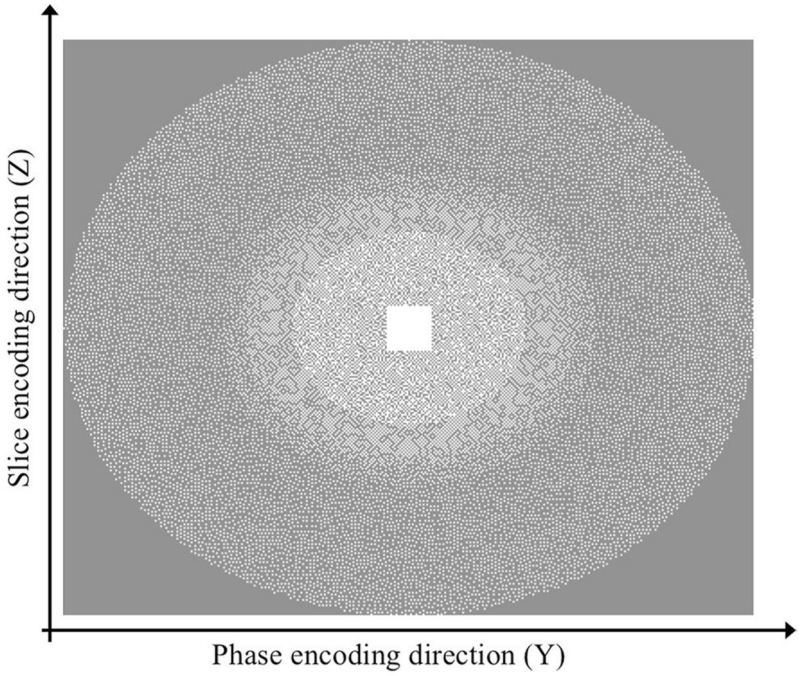

Fig. 1.

The *k*-space sampling pattern used in CS-SPACE. A variable density Poisson disc distribution was used in the kz–ky plane in 3D MR imaging with a 24 × 24 fully sampled region around the *k*-space center. No undersampling was done along the readout direction

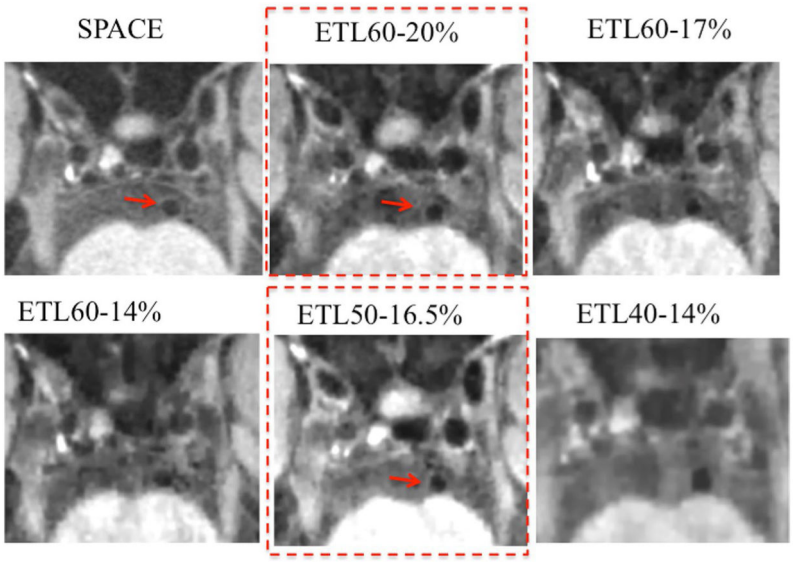

Fig. 2.

Optimization of acquisition parameters in a volunteer. Middle slice of the basilar artery is shown. Optimized protocols are shown in the boxes. Arrows show basilar artery wall

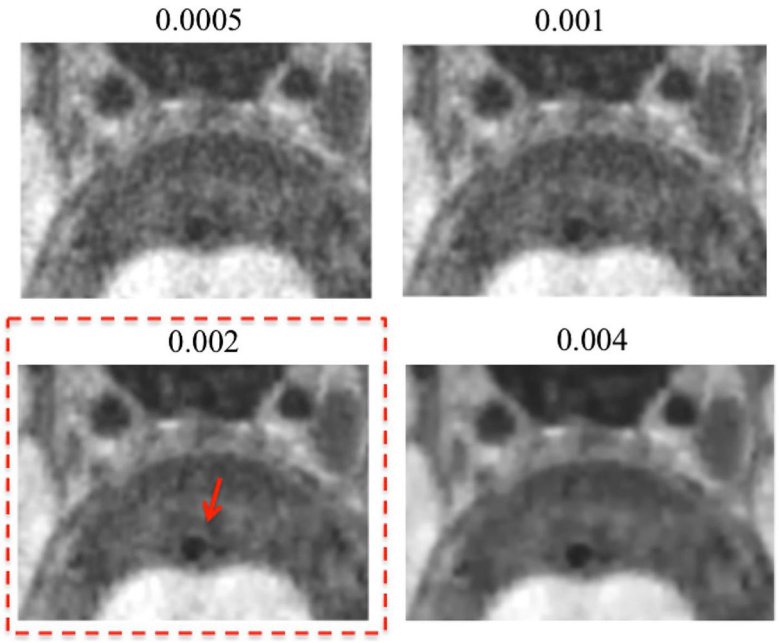

Fig. 3.

Optimization of regularization parameter in a volunteer's basilar artery. Optimized regularization parameter is shown in the box. Arrow shows the basilar artery wall

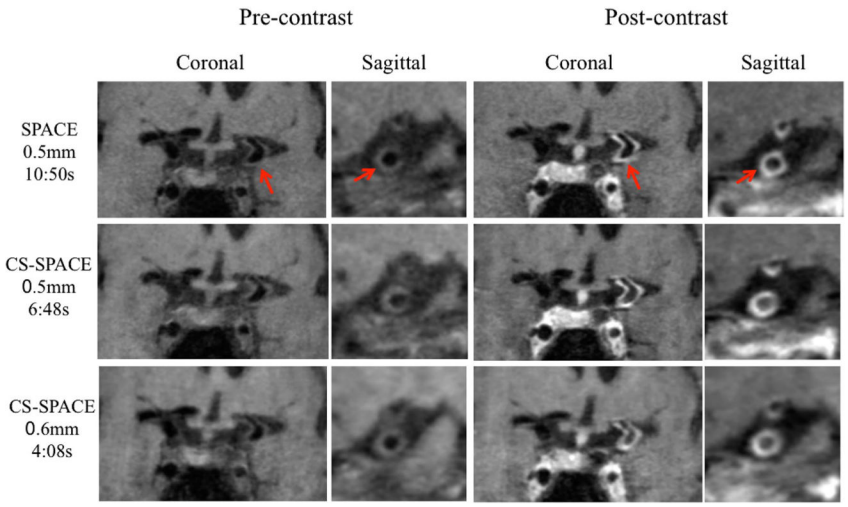

Fig. 4.

A patient with vasculitis. Post-contrast images show strong circumferential enhancement of the left internal carotid artery and left middle cerebral artery. Arrows show the vessel wall and enhancement. All three protocols can identify vessel wall and enhancement clearly. CS-SPACE 0.6 mm images have slightly lower image quality due to decreased resolution

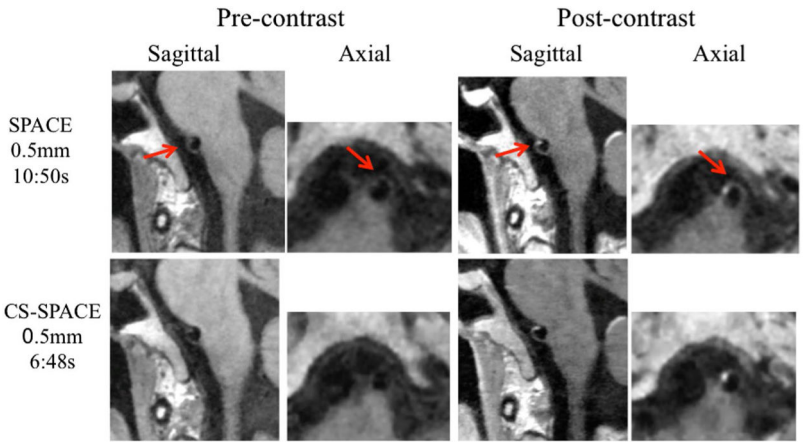

Fig. 5.

A patient with vertebral artery dissection. Arrows show vertebral artery wall and enhancement. Both protocols can identify vessel wall and enhancement clearly. Note the degraded image quality in axial plane compared with sagittal plane

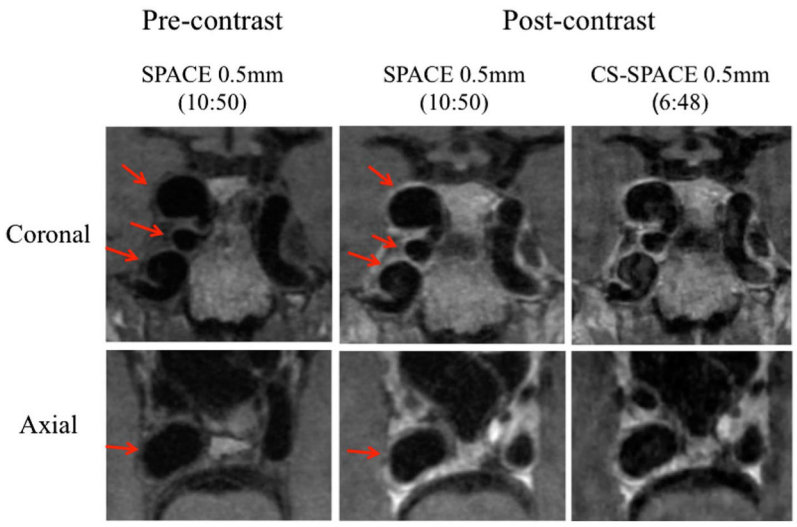

Fig. 6.

A patient with 3 ICA aneurysms. Arrows show aneurysm wall and enhancement. Both protocols can identify vessel wall and enhancement clearly

Table 1

Scanning parameters

	SPACE	ETL60-20%	ETL60-17%	ETL60-14%	ETL50-16.5%	ETL40-14%
Scan time	10:50	6:48	5:57	4:31	6:43	6:45
Reduced time%[a]	N/A	37.2%	45.1%	58.3%	38.0%	37.7%
k-Space under sampling (acceleration)	31.8%[b] (*R* = 3.1)	20% (*R* = 5.0)	17% (*R* = *R* = 5.9)	14% (*R* = 7.1)	16.5% (*R* = 6.1)	14% (*R* = 7.1)
FOV	18 cm	19.2 cm				
Matrix	360 × 360	384 × 384				
ETL	60				50	40
TR/TE	1000 ms/17 ms					
Acquisition orientation	Sagittal					
Slices	320					

FOV filed of view, *ETL* echo train length

[a]Compared with conventional SPACE

[b]Conventional SPACE used GRPAA 2 in phase encoding direction, 6/8 partial Fourier in slice direction, and elliptical *k*-space sampling

Table 2

Qualitative image scores of different CS-SPACE protocols and SPACE images in volunteers ($n = 5$)

	SPACE	ETL60-20%	ETL60-17%	ETL60-14%	ETL50-16.5%	ETL40-14%	*p* value
Scan time	10:50	6:48	5:57	4:31	6:43	6:45	
Image score	3.46 ± 0.76	3.08 ± 0.57[a]	3.06 ± 0.70	2.54 ± 1.01	3.14 ± 0.65*	3.00 ± 0.79	< 0.001
MCA (sagittal)	3.60 ± 0.84	3.50 ± 0.53	3.70 ± 0.48	3.40 ± 0.70	3.60 ± 0.70	3.70 ± 0.48	0.38
ICA (mean)	3.45 ± 0.69	2.80 ± 0.42	2.75 ± 0.35	2.15 ± 0.41	2.85 ± 0.41	2.70 ± 0.35	< 0.001
ICA (sagittal)	3.78 ± 0.67	3.33 ± 0.50	3.11 ± 0.33	2.89 ± 0.60	3.56 ± 0.53	3.67 ± 0.50	0.01
ICA (axial)	3.44 ± 0.53	2.33 ± 0.71	2.44 ± 0.53	1.44 ± 0.53	2.22 ± 0.44	1.78 ± 0.44	< 0.001
BA (axial)	3.20 ± 0.84	2.80 ± 0.45	2.40 ± 0.55	1.60 ± 1.14	2.80 ± 0.45	2.20 ± 0.84	0.045

[a]Optimized imaging scores of CS-SPACE

Table 3

Quantitative measurements of different CS-SPACE protocols and SPACE images in volunteers (n = 5)

	SPACE	ETL60-20%	ETL60-17%	ETL60-14%	ETL50-16.5%	ETL40-14%	*p* value
Scan time (reduction%)	10:50	6:48 (37.2%)	5:57 (45.1%)	4:31 (58.3%)	6:43 (38.0%)	6:45 (37.7%)	
Lumen area (ICC[a])	10.1 ± 4.9	9.7 ± 4.1 (0.87)	10.6 ± 5.2 (0.87)	9.8 ± 5.1 (0.80)	10.0 ± 4.4 (0.87)	10.2 ± 4.7 (0.86)	0.18
Outer area (ICC[a])	22.6 ± 9.8	22.2 ± 8.6 (0.90)	25.6 ± 11.8 (0.80)	25.0 ± 10.7 (0.81)	22.8 ± 8.7 (0.88)	24.9 ± 10.0 (0.84)	< 0.001
Wall area (ICC[a])	12.5 ± 5.4	12.5 ± 4.9 (0.89)	14.9 ± 7.4 (0.66)	15.3 ± 6.9 (0.68)	12.8 ± 4.9 (0.80)	14.7 ± 6.3 (0.73)	< 0.001
Average ICC	NA	0.89[b]	0.78	0.76	0.85	0.81	
Contrast ratio	1.88 ± 0.33	2.07 ± 0.35	2.00 ± 0.35	2.00 ± 0.37	2.11 ± 0.44	2.01 ± 0.34	0.007

[a] ICC represents the agreement between measurements from CS-SPACE and SPACE

[b] Optimized ICC value

Table 4

Qualitative image scores of SPACE and CS-SPACE in patients

	Reader 1	Reader 2
SPACE pre	3.23 ± 0.83	3.46 ± 0.88
CS-SPACE pre	3.38 ± 0.77	3.69 ± 0.48
p values	0.63	0.25
SPACE post	3.56 ± 0.73	3.88 ± 0.54
CS-SPACE post	3.63 ± 0.62	3.44 ± 0.51
p values	1.00	0.06
SPACE pre + post	3.41 ± 0.78	3.69 ± 0.66
CS-SPACE pre + post	3.52 ± 0.69	3.42 ± 0.51
p values	0.51	0.34

Table 5

Quantitative measurements comparison between SPACE and CS-SPACE images in patients (from 16 lesions, mixed pre- and post-contrast)

	SPACE	CS-SPACE	*p* value	ICC (95% CI)
Lumen area (mm^{-1})	22.5 ± 31.4	23.3 ± 33.7	0.40	0.993 (0.989, 0.996)
Wall area (mm^{-1})	23.0 ± 17.4	23.4 ± 16.0	0.51	0.967 (0.947, 0.980)
Wall/lumen contrast ratio	2.26 ± 0.85	2.09 ± 0.63	0.02	N/A
Enhance ratio	1.44 ± 0.46	1.47 ± 0.42	0.47	0.897 (0.787, 0.952)
Sharpness-inner boundary (mm^{-1})	1.71 ± 0.58	1.73 ± 0.61	0.91	N/A
Sharpness-outer boundary (mm^{-1})	2.16 ± 0.73	2.12 ± 0.70	0.73	N/A
Sharpness-mean (mm^{-1})	1.94 ± 0.47	1.92 ± 0.48	0.83	N/A